Catalytic Effects of Photogenerated Fe(II) on the Ligand-Controlled Dissolution of Iron(hydr)oxides by EDTA and DFOB

Jagannath Biswakarma[1,2], Kyounglim Kang[3], Walter D.C. Schenkeveld[4], Stephan M. Kraemer[3], Janet G. Hering[1,2,5] and Stephan J. Hug[2]*

[1] Swiss Federal Institute of Technology (ETH) Zurich, IBP, CH-8092 Zürich, Switzerland

[2] Eawag, Swiss Federal Institute of Aquatic Science and Technology, CH-8600 Dübendorf, Switzerland

[3] University of Vienna, Dept. of Environmental Geosciences, 1090 Vienna, Austria

[4] Copernicus Institute of Sustainable Development, Faculty of Geosciences, Utrecht University, 3584 CB Utrecht, the Netherlands

[5] Swiss Federal Institute of Technology Lausanne (EPFL), ENAC, CH-1015 Lausanne, Switzerland

* Corresponding author. E-mail: stephan.hug@eawag.ch

Highlights

- Photogenerated Fe(II) accelerates ligand-controlled dissolution of Fe(III)oxides
- Dissolution with DFOB or EDTA is accelerated up to 40-fold under anoxic conditions
- Short illuminations (5-15 min) lead to continued dissolution in the dark
- Photoinduced dissolution under oxic conditions requires photostable ligands
- Even short exposures to sunlight might lead to increased bioavailability of iron

Graphical Abstract

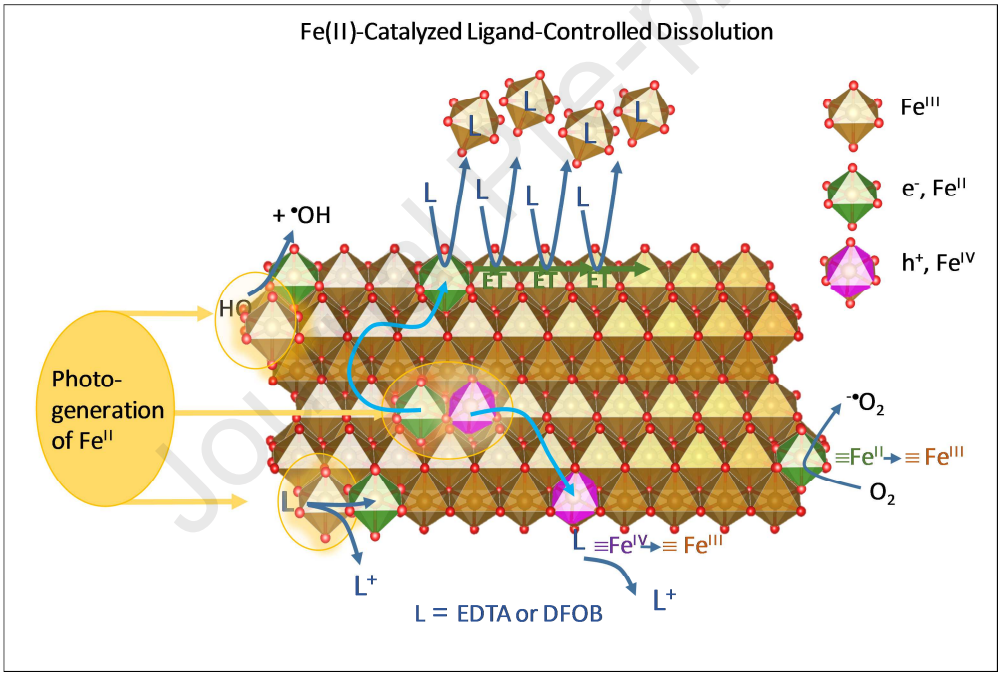

Abstract

Low bioavailability of iron due to poor solubility of iron(hydr)oxides limits the growth of microorganisms and plants in soils and aquatic environments. Previous studies described accelerated dissolution of iron(hydr)oxides under continuous illumination, but did not distinguish between photoreductive dissolution and non-reductive processes in which photogenerated Fe(II) catalyzes ligand-controlled dissolution. Here we show that short illuminations (5-15 min) accelerate the dissolution of iron(hydr)oxides by ligands during subsequent dark periods under anoxic conditions. Suspensions of lepidocrocite (Lp) and goethite (Gt) (1.13 mM) with 50 µM EDTA or DFOB were illuminated with UV-A light of comparable intensity to sunlight (pH 7.0, bicarbonate-CO_2 buffered solutions). During illumination, the rate of Fe(II) production was highest with Gt-EDTA; followed by Lp-EDTA > Lp-DFOB > Lp > Gt-DFOB > Gt. Under anoxic conditions, photochemically produced Fe(II) increased dissolution rates during subsequent dark periods by factors of 10-40 and dissolved Fe(III) reached 50 µM with DFOB and EDTA. Under oxic conditions, dissolution rates increased by factors of 3-5 only during illumination. With DFOB dissolved Fe(III) reached 35 µM after 10 h of illumination, while with EDTA it peaked at 15 µM and then decreased to below 2 µM. The observations are explained and discussed based on a kinetic model. The results suggest that in anoxic bottom water of ponds and lakes, or in microenvironments of algal blooms, short illuminations can dramatically increase the bioavailability of iron by Fe(II)-catalyzed ligand-controlled dissolution. In oxic environments, photostable ligands such as DFOB can maintain Fe(III) in solution during extended illumination.

1. Introduction

Dissolution of Fe(III)(hydr)oxides is one of the key processes in the biogeochemical Fe cycle and may govern the (bio)availability of Fe in the environment. Suspended Fe(III)(hydr)oxide particles in surface waters are important sources of Fe to microorganisms, but under oxic conditions their low solubility and slow dissolution kinetics can lead to Fe deficiency. To acquire Fe, organisms excrete ligands that promote the dissolution of Fe(III)(hydr)oxides. In sunlit waters, photochemical reactions lead to reduction of particulate Fe(III) to soluble and bioavailable Fe(II), for example in surface water (Waite and Morel, 1984; Sulzberger and Laubscher, 1995b; Voelker et al., 1997), seawater (Wells et al., 1991; Johnson et al., 1994; Kuma et al., 1995), atmospheric water (Faust and Hoigne, 1990; Faust and Zepp, 1993; Pehkonen et al., 1993; Fu et al., 2010), and ice (Kim et al., 2010b). Laboratory and field studies have demonstrated that solar and UV light induces photoreductive dissolution of Fe(III)(hydr)oxides in the presence of ligands secreted by marine phytoplankton and algae, and by terrestrial microbes and plants (Litter et al., 1991; Goldberg et al., 1993; Barbeau et al., 2003; Kraemer et al., 2005). Our recent studies have shown that traces of Fe(II) can catalyze the overall non-reductive dissolution of a range of Fe(III)(hydr)oxides in the presence of ligands (Biswakarma et al., 2019; Kang et al., 2019; Biswakarma et al., 2020). Sunlight might thus accelerate the dissolution of Fe(III)(hydr)oxide not only by photoreductive dissolution, but in addition by Fe(II)-catalyzed ligand-controlled dissolution. Short intermittent illuminations might be sufficient to lead to rapid dissolution, without much reduction of Fe(III) to Fe(II).

In the presence of ligands, photoreductive dissolution of Fe(III)(hydr)oxides can be explained by two possible processes, which can also occur in parallel. In the first process, due to the intrinsic photoreactivity of Fe(III)(hydr)oxides, light absorbed by the solids causes photoinduced charge separation in the bulk with formation of mobile electrons and electron holes (Sherman, 2005; AlSalka et al., 2019). These charges can recombine or migrate to the surface where they form Fe(II) and Fe(IV) or $^{\bullet}OH$ (Sherman, 2005). A smaller fraction of light absorbed on the surface also leads to formation of Fe(II) and $^{\bullet}OH$ on the surface by ligand-to-metal charge transfer (LMCT) from surface hydroxyl groups to surface Fe(III). In the absence of ligands, most of the formed surface Fe(IV), Fe(II) and $^{\bullet}OH$ react back to surface Fe(III) and hydroxyl groups, which results in only low yields of Fe(II) and products such as H_2O_2. Adsorbed ligands can act as scavengers for surface Fe(IV) or $^{\bullet}OH$, leading to

accumulation of Fe(II) and oxidation products of the ligand on the surface. In the second process, absorption of light by Fe(III)-ligand surface complexes induces LMCT from ligands to the surface, with formation of Fe(II) and oxidation products of the ligand (Waite, 1990; Barbeau et al., 2003; Borer et al., 2009c; Borowski et al., 2018). In previous studies, dissolved Fe(II) and total dissolved Fe were quantified while mineral suspensions were continuously exposed to solar or UV illumination (Borer et al., 2005; Borer et al., 2007, 2009a; Borer and Hug, 2014). Rates of photoreductive dissolution in the presence of ligands during illumination were reported to be higher than ligand-controlled dissolution rates in the dark, and explained by faster detachment of Fe(II) by ligands than of Fe(III) (Litter and Blesa, 1988; Goldberg et al., 1993; Karametaxas et al., 1995; Sulzberger and Laubscher, 1995a). However, the possibility that photogenerated Fe(II) also accelerates the detachment of Fe(III) by ligands and that this effect could persist even after illumination ceased was not investigated.

In recent studies (Biswakarma et al., 2019; Kang et al., 2019; Biswakarma et al., 2020), we examined the effect of added Fe(II) on the dissolution of Fe(III)(oxyhydr)oxides and found that micromolar concentrations of Fe(II) lead to up to a 60-fold acceleration of dissolution rates under anoxic conditions. We further demonstrated that photochemically formed Fe(II) accelerates dissolution rates of lepidocrocite with EDTA under anoxic conditions, but not under oxic conditions.

Here, we extend our previous work by quantifying photoproduced Fe(II) and its effect on the dissolution of lepidocrocite (Lp) and goethite (Gt) with the synthetic ligand EDTA and with the biogenic siderophore desferrioxamine B (DFOB). Dissolved complexes of Fe(III) with EDTA are photoreactive and form Fe(II) with a quantum yield of 0.034 at 365 nm (Kari et al., 1995), while dissolved complexes of Fe(III) with DFOB are not photoreactive (Kunkely and Vogler, 2001; Rijkenberg et al., 2006). The goal was to investigate how much Fe(II) can be produced photochemically in suspensions of Lp and Gt at circumneutral pH in the absence and presence of ligands and how Fe(II) affects ligand-controlled dissolution rates after intermittent and during continuous illumination under anoxic and oxic conditions.

As pH and carbonate concentrations strongly affect the speciation and sorption of Fe(II), we extended the pH range from 6.0 to 8.5 and performed experiments at pH 7.0 in carbonate-CO_2 buffered suspensions to mimic environmental conditions. Experiments were performed under anoxic and oxic conditions and at pH 6.0 (MES buffered), 7.0 (CO_2-carbonate buffered) and 8.5 (PIPES-buffered). In

contrast to our previous, *in situ* attenuated total reflectance fourier-transformed infrared (ATR-FTIR) studies with Lp and EDTA, (Biswakarma et al., 2019) we conducted batch dissolution experiments with Lp, Gt, EDTA and DFOB under both intermittent (5 or 15 min) and continuous illumination.

2. Experimental Section

2.1. Materials

All chemicals used were of analytical grade and are listed in the Supplementary Material Table S1. Aqueous solutions were prepared using high-purity doubly-deionized (DDI) water (Barnstead Nanopure). The BET (N_2 Brunauer−Emmett−Teller) specific surface areas were 63 m^2/g for Lp and 105 m^2/g for Gt. The synthesis and characterization of Lp and Gt were described in our recent studies (Biswakarma et al., 2019; Kang et al., 2019).

2.2. Photochemical Experiments

Suspensions of Lp and Gt with EDTA or DFOB (100 ml) were irradiated in 120 ml Pyrex bottles with UV-A light in a box with 8 Philips TL20W/05 (actinic blue) lamps. The lamps have a broad emission spectrum from 300-450 nm (maximum at 365 nm) and closely simulate solar illumination in the UV-A spectral range (Hug et al., 2001). The emission spectrum of the UV-source and the spectra of Lp, Fe(III)EDTA and Fe(III)DFOB are shown in Fig. S1. All experiments were conducted at room temperature (23-24 ºC). Increases in temperature in the box with the UV-lamps were limited <1 ºC during intermittent illuminations to < 3ºC during continuous illumination by a strong ventilator induced flow of air.

2.3. Photon flux

The photon flux entering the Pyrex bottles (320-450 nm) was measured by ferrioxalate actinometry (Hatchard and Parker, 1956).100 ml of a 6 mM ferrioxalate actinometer solution absorbed all incoming light of our UV-A light source. The light flux was determined as 1.37 µmol photons/s, which is comparable to the light flux of 1.63 µmol photons/s measured when the actinometer was

exposed to sunlight on a clear day (11:30 am, November 7, 2018). Over 99% of the light in this spectral range was absorbed by the 1.13 mM suspensions of Lp and Gt (Fig. S1).

2.4. Photoproduction of Fe(II)

The photoproduction of Fe(II) was measured at pH 7.0 under anoxic conditions, by adding 470 µM phenanthroline (phen) to the Lp or Gt suspensions (without and with 50 µM EDTA or DFOB). We assume that with the large excess of phen, all photochemically formed Fe(II) forms dissolved $Fe(II)(phen)_3^{2+}$ complexes. This is supported by speciation calculations which show that Fe(II) in the presence of 50 µM EDTA or DFOB and 470 µM phen is complexed to over 99.9% as $Fe(II)(phen)_3^{2+}$ at pH 6.0-8.0 (Fig. S2). $Fe(II)(phen)_3^{2+}$ in filtered samples was quantified by measuring UV-spectra and calculation of concentrations from the absorbance at 510 nm ($\varepsilon_{510\ nm}$ = 11000 $M^{-1}cm^{-1}$), see Fig. S3. (The detection limit was 0.0005 absorbance units at 510 nm (average of 11 data points from 505-515 nm) corresponding to 0.05 µM $Fe^{II}(phen)_3^{2+}$).

2.5. Formation of FeEDTA and FeDFOB in suspensions of Lp and Gt

All experiments were conducted with initially 100 ml suspensions containing 100 mg/L (1.13 mM) FeOOH (Lp or Gt) and 50 µM EDTA or DFOB. For the experiments at pH 7.0, the background electrolyte was 3 mM $NaHCO_3$; before and during illumination, suspensions were continuously purged with a mixture of 2% CO_2 in N_2 (anoxic) or 2% CO_2 in air (oxic). Experiments at pH 6.0 (9.5 mM NaCl and 5 mM MES) and at pH 8.5 (9.5 mM NaCl and 5 mM PIPES) were sparged with N_2 (anoxic) or synthetic air (oxic). Suspensions were irradiated either continuously or intermittently; the periods of intermittent illumination were typically 5 min for experiments with EDTA (unless mentioned otherwise in the text or figure captions) and 15 min for experiments with DFOB. Samples were withdrawn periodically with a syringe and immediately filtered through 0.1 µM Nylon filters. Subsequently, UV-VIS spectra (200-800 nm) were measured to quantify the formed Fe(III)EDTA or Fe(III)DFOB complexes in 1 cm path-length quartz cuvettes. Examples of measured spectra and of data processing are shown in Fig. S4 and S5. Note that with this method, we measure the sum of Fe(II) and Fe(III) complexes, as both Fe(II)EDTA and Fe(II)DFOB were quickly oxidized in the cuvettes upon contact with air. We thus refer to dissolved iron as $[Fe]_{diss}$ in the figures and in the discussion of the experiments. In the course of dissolution during dark periods, concentrations of Fe(III)EDTA or

Fe(III)DFOB dominate over the Fe(II) species, because less than 3 µM of Fe(II) was produced during intermittent UV-illuminations. In the oxic experiments, all dissolved Fe(III) was present as Fe(III)EDTA or Fe(III)DFOB.

Most experiments at pH 6.0 and pH 7.0 were repeated at least two times, but samples were not always withdrawn at the same time. Differences between repeated experiments were less than 10 % for data points measured at the same times, as shown in Fig. S6. In the figures in the manuscript, we add error bars of ± 5% for each data point. Since each experiment consists of a series of 12-24 connected data points, the exact error range of each individual data point is not critical for the discussion of the results, as illustrated by the kinetic model fits, which fall within the error bars.

2.6. Kinetic Model

To test if the later suggested reaction sequences are able to explain the experimentally measured data, we performed kinetic modeling similar to our previous studies. We used the kinetic program Acuchem (Braun et al., 1988) in combination with Matlab (MATLAB, MathWorks, Inc., Natick, Massachusetts, www.mathworks.com). To model experiments with changing conditions (successive dark and light periods) model fits had to be calculated in several segments, with the end concentrations of each segment carried over to the next segment as starting concentrations. The input of starting concentrations and the optimization of unknown rate coefficients was achieved by using Acuchem under the control of Matlab.

3. Results

3.1. Photochemical Formation of Fe(II) in Lp and Gt Suspensions without and with Dissolution-Promoting Ligands

The photochemical formation of Fe(II), measured with a large excess of phen (470 µM) in suspensions of Lp and Gt without and with EDTA or DFOB is shown in Fig. 1. Stable concentrations of $Fe(II)(phen)_3^{2+}$ (changing less than 5% in 5 min) were reached within 5-10 min after each illumination, as shown for Lp in the presence of DFOB in Fig. S3. As shown in Fig. 1, the concentration of $Fe(II)(phen)_3^{2+}$ in suspensions of either Lp and Gt increased linearly as a function of

the total duration of illumination. This linear increase confirms that the low concentrations of Fe(II)$(phen)_3^{2+}$ formed in our experiments did not lead to significant light absorption or interactions with Lp or Gt. Also, phen did not lead to reduction of lepidocrocite or goethite; as shown for Lp in Fig. S3; Fe(II) was only detected after illumination. ATR-FTIR experiments conducted at pH 6.0 (Fig. S7) confirmed that phen did not measurably adsorb to the surface of Lp or lead to changes in the IR-spectra of adsorbed EDTA. The photoreactivity of EDTA in the presence of phen was not different than in the absence of phen according to our previous observations (Biswakarma et al., 2019). Since both EDTA and DFOB adsorb strongly to Lp and Gt at pH 6.0 and 7.0, and the speciation of phen does not change in this pH range, we assume that phen does also not interfere with the adsorption and photoreactions of EDTA and DFOB on the surface of Gt. The rates of photochemical Fe(II) formation were determined from the slopes of the linear fits as indicated in Fig. 1 and as listed in Table 1a.

In the absence of the dissolution-promoting ligands EDTA or DFOB, 0.10 μM Fe(II)$(phen)_3^{2+}$ was measured after Gt was exposed to 15 min of illumination, corresponding to a maximum rate of photochemical Fe(II) formation of 0.006 μM/min. This value was substantially higher with Lp, consistent with the intrinsic photochemical activity of Lp ascribed to light absorption in the bulk and formation of mobile charge carriers and Fe(II) and OH-radicals on the surface, as reported previously (Borer et al., 2009c).

The presence of EDTA and DFOB increased the rates of photochemical Fe(II) formation for both solids. The most significant enhancement was observed for Gt in the presence of EDTA; addition of EDTA increased the rate of photochemical Fe(II) formation by a factor of ~90 in comparison with the solid alone, while the increase with DFOB was only a factor of 1.7. For Lp, the rate of photochemical Fe(II) formation increased by a factor of 5.4 by EDTA, but only by a factor of 2.3 by DFOB.

The pronounced effects with EDTA may be due to the high photoreactivity of EDTA surface complexes or to efficient hole scavenging by adsorbed EDTA. In order to produce comparable concentrations of around 2.5 μM Fe(II) in subsequent Lp dissolution experiments, we applied intermittent illumination periods of 5 min for EDTA and of 15 min for DFOB (see Table 1).

3.2. Effect of UV-A Illumination on Lp Dissolution

3.2.1. In the presence of EDTA.

Fig. 2 shows the measured concentrations of total dissolved Fe ($[Fe]_{diss.}$) in Lp suspensions in the presence of EDTA as a function of time at pH 6 and 7 under anoxic and oxic conditions. The thin black lines show the output of the kinetic model described later in the discussion section. Note that all dissolved Fe is assumed to be complexed by EDTA (see Materials and Methods). Initially the reaction was allowed to proceed without any UV illumination for 90 min. During this initial period, Lp dissolution was very slow under all conditions (see Table 1b for rates), in good agreement (± 20 % relative difference) with the rates reported in our previous study (Biswakarma et al., 2019). Dissolution rates of our previous studies are listed in SI, Table S2.

Anoxic suspensions were exposed to a single, illumination period of five minutes (90-95 min). At both pH 6 and 7, a distinct increase in $[Fe]_{diss.}$ was observed immediately after the illumination period (no samples were collected during illumination). Continued rapid increases in $[Fe]_{diss.}$ were observed after illumination, indicating the continuation of accelerated dissolution of Lp. At pH 6, the reaction reached completion within 150 min; $[Fe]_{diss}$ (orange squares in Fig. 2) approaching the total concentration of EDTA (50 µM). At pH 7, $[Fe]_{diss.}$ increased more slowly (orange triangles in Fig. 2), but accelerated dissolution also persisted after illumination and the concentration of dissolved Fe reached 50 µM after 420 min.

Dissolution rates (Table 1b) were computed from linear regression lines as shown in the figures. In the presence of EDTA at pH 7, the rate of Lp dissolution was 8 times faster after illumination than before it. The accelerated dissolution rate at pH 7 persisting after the cessation of illumination under anoxic conditions was expected with the photochemical production of 2.15 µM Fe(II) in Lp suspensions with 50 µM EDTA as measured in the presence of a large excess of phen (Fig. 1). At pH 6, the rate of Lp dissolution was 33 times faster after 5 min intermittent illumination than before it. Observations under continuous illumination (purple triangles) can provide insights into important differences between the effects of intermittent and continuous illumination. Under anoxic conditions, at pH 7.0, $[Fe]_{diss}$ increased rapidly and nearly linearly at a rate 27 times faster than prior to illumination, but only to a final concentration of 43 µM. Apparently, some of the EDTA was photo-degraded during continuous illumination under anoxic conditions consistent with previous

observations (Karametaxas et al., 1995), while only minimal degradation occurred during short intermittent illumination periods.

Under oxic conditions at both pH 6 and 7 (Fig. 2), intermittent illuminations resulted in slight increases in $[Fe]_{diss.}$ at the end of the illumination period, but further dissolution was not significantly accelerated compared to that prior to illumination. The increase in $[Fe]_{diss.}$ during illumination is consistent with our prior *in situ* observation of accelerated Lp dissolution during illumination under oxic conditions (Biswakarma et al., 2019), which also showed no persistence of the accelerated dissolution subsequent to illumination. Adsorbed Fe(II) and dissolved complexed Fe(II)EDTA are known to be oxidized quickly by dissolved oxygen (Karametaxas et al., 1995; Kari et al., 1995).

3.2.2. In the presence of DFOB

Fig. 3 shows the results of comparable experiments (conducted at pH 7 and 8.5) with DFOB instead of EDTA. The thin black lines show the output of kinetic modeling. Before illumination, $[Fe]_{diss.}$ increased only slowly and at the same rates (Table 1b) under anoxic (orange) and oxic (blue) conditions. The dark dissolution rate was 2 times faster at pH 8.5 than at pH 7.0. The dissolution rates in the dark are in reasonable agreement with our previously-reported values (Biswakarma et al., 2019) (see Table S2).

Under anoxic conditions, intermittent UV-illumination periods led to accelerated Lp dissolution that persisted in the dark. At pH 7, $[Fe]_{diss}$ (orange circles) reached 50 µM in 450 min in response to three intermittent 15 min illuminations, corresponding to a ca. 9-fold increase in the dissolution rate. Our measurements with phen indicate that 2.7 µM of Fe(II) were produced during each 15 min illumination. In our previous study,[19] addition of 1 µM Fe(II) resulted in an 18-fold increase in Lp dissolution rate in the presence of DFOB. As the effect with added Fe(II) is larger than in the photochemical experiments, it is possible that photogenerated Fe(II) is partially oxidized due to concurrent formation of oxidants such as H_2O_2. Additionally, Fe(II) can be oxidized due to the instability of Fe(II)DFOB complexes, which are reported to slowly auto-decompose with formation of Fe(III) and a DFOB monoamide (Kim et al., 2009, 2010a). Under continuous illumination at pH 7.0 under anoxic conditions without prior intermittent illumination (orange open circles), the Lp dissolution rate was accelerated by a factor of 16 (nearly twice that observed after intermittent

illumination). At pH 8.5, nearly-linear Lp dissolution continued after the first 15-min UV illumination at a rate 2-fold the initial dissolution rate (prior to UV illumination) (Table 1b).

Under oxic conditions, reliable estimates of accelerated dissolution rates could be obtained only under continuous illumination. This was examined only for pH 7, where a 5.5-fold increase in the dissolution rate was observed. This dissolution rate is roughly consistent with the changes in $[Fe]_{diss.}$ observed after intermittent illumination.

3.2.3. EDTA *vs* DFOB (anoxic)

A comparison of the effects of EDTA and DFOB for single intermittent UV illuminations of 5 and 15 min at pH 7 is shown in Fig. S8. For both illumination periods, the effect with EDTA was larger than the effect with DFOB; this is particularly noticeable when the illumination period is the same for both ligands.

3.2.4. EDTA *vs* DFOB (Oxic)

Since dissolution under oxic conditions is more easily assessed during continuous illumination, we conducted such experiments with EDTA and DFOB at pH 7. In Fig. 4, results with EDTA are shown together with the results with DFOB. With EDTA, $[Fe]_{diss.}$ reached a maximum value of 15 µM after 240 min and then decreased, suggesting photolysis of dissolved Fe(III)EDTA, which is reported to occur with quantum yields of 0.034-0.018 from 366-405 nm (Kari et al., 1995), and of EDTA surface complexes (Biswakarma et al., 2019). In contrast to EDTA, $[Fe]_{diss}$ in the presence of DFOB did not reach a maximum value and decline afterwards. The Lp dissolution rate under continuous illumination (initially 5.5-fold faster than the rate without UV illumination) appears to slow down after 480 min with $[Fe]_{diss}$ reaching a plateau at ca. 35 µM DFOB and EDTA appear to have similar effects on Lp dissolution under continuous illumination, initially; the persistence of the accelerated Fe dissolution with DFOB, but not with EDTA is consistent with the fact that DFOB is a more photostable ligand than EDTA (Borer et al., 2009b; Borer et al., 2009c). Although DFOB appears to be able to complex Fe(III) over time periods of hours in irradiated solutions, the decrease in dissolution rate and the eventual plateau in $[Fe]_{diss}$ suggests that Fe(II) may react with oxidants accumulated during the

illumination (e.g. H_2O_2) (Borer et al., 2009c) and/or that DFOB may undergo some photodegradation over longer periods or illumination.

As discussed above, the effects of intermittent illumination under oxic conditions are difficult to assess. Additional experiments with both EDTA and DFOB (Fig. S9) showed only inconsistent effects.

3.3. Effect of UV-A Illumination on Gt Dissolution

Fig. 5 shows Gt dissolution at pH 7 in the presence of EDTA and DFOB before and after intermittent illuminations. Before illumination, Gt dissolution was very slow (R = 0.01% hr^{-1} with EDTA, and not detectable with DFOB). Intermittent illumination under anoxic conditions with EDTA resulted in a increase in $[Fe]_{diss.}$ during illuminations (open orange triangles) and accelerated dissolution persisted after illumination ceased. The accelerating effect was roughly 36-fold (average of three rates) for each of the three intermittent illumination periods (Table 1b). In contrast, intermittent illumination of Gt in the presence of DFOB had no measurable effect under anoxic conditions (open orange circles) or oxic conditions (data not shown).

Under oxic conditions with EDTA, the first intermittent illumination (5 min) appeared to result in a small step-increase in $[Fe]_{diss.}$ (open blue triangles), but no persistent accelerated dissolution was observed and even the step-increase was not observed in subsequent intermittent illuminations.

3.4. Contrasting Photochemical Properties of Lp and Gt under Anoxic Conditions

Because the ligand-controlled (i.e., dark) dissolution rate of Gt was so much smaller than that of Lp, the largest effect of intermittent illumination was observed with Gt/EDTA (average 36-fold acceleration). For Lp dissolution, the enhancement with EDTA (under intermittent illumination) was a factor of 8 (see Fig. S10). This difference cannot be explained by the photoproduction of Fe(II) since this was nearly the same for both solids: 2.70 µM for Gt and 2.15 µM for Lp in 5 min of illumination (Table 1). The lack of any detectable effect of intermittent illumination with DFOB and Gt is consistent with the negligible Fe(II) photoproduction (0.15 µM over 15 min).

3.5. Phase Transformations

No transformation of Lp to other Fe(III) phases, such as Gt or magnetite (Mgt), was detected after 480 min continuous illumination of Lp in the presence of either EDTA or DFOB, by ATR-FTIR spectroscopy (Fig. S11). As explained in the caption of Fig. S11, we estimate detection limits for Gt and Mgt in Lp of < 3% with ATR-FTIR. However, we cannot exclude formation of smaller fractions of Mgt, particularly at pH 8.5. With our experimental set-up, we could not collect sufficient amounts of solids for XRD measurements. The photoinduced formation of small fractions of Mgt or other phases (e.g. green rusts) as a function of pH and illumination time could be the subject of future studies.

4. Discussion

4.1. Reaction Mechanisms, Rates of Light Absorption, Quantum Yields, and Kinetic Model

4.1.1. Catalytic effect of Fe(II)

Table 2a lists the main reactions for the photochemical formation of Fe(II) and for Fe(II)-catalyzed dissolution with DFOB and EDTA. Both ligands are abbreviated as L. Note that surface hydroxyl groups, the modes of coordination of ligands to the surface, and the transfer and balance of oxo- and hydroxyl oxygens are not specified in the listed reactions. Also, for simplicity, we do not specify the protonation and charges of the ligands and their complexes with iron. There are several differently protonated and charged species of each reactant; accounting for all species is not possible because the charges and protonation of surface complexes are not known.

The reactions in Table 2a were used for the kinetic modeling of the data measured at pH 7.0. Some of the reactions that apply to EDTA are described in more detail in Table 2b. Similar reactions as for EDTA apply for DFOB, with the difference that reaction products are different and that dissolved Fe(III)DFOB complexes are photochemically inactive (Kunkely and Vogler, 2001; Barbeau et al., 2003)' (Borer et al., 2005; Borer et al., 2009a; Borer et al., 2009b). DFOB surface complexes are much

less photoreactive than surface complexes of ligands that adsorb to Lp and Gt by coordination of carboxylate groups, but some photoactivity of adsorbed DFOB ascribed to photoinduced LMCT has been observed at pH 8.0 during illumination with light in the 395-435 nm wavelength range (Borer et al., 2009d).

In the absence of Fe(II), ligand-controlled dissolution is slow (R1a-R1c). When Fe(II) and oxidants are photochemically formed on the surface (R2a-h), or Fe(II) is adsorbed from solution (R3), dissolution becomes fast (R4a), facilitated by electron transfer (ET) from surface Fe(II) complexed to the ligand to a neighboring site on the surface and faster detachment of Fe(III)L due to weaker Fe(II)-O bonds to the lattice compared to Fe(III)-O bonds in the absence of Fe(II). Additional reactions, such as adsorption of Fe(II)L to surface Fe(III) sites (R4b) and adsorption of Fe(II) to adsorbed ligands (R4c), followed by ET and subsequent detachment of Fe(III)L, can contribute to rapid Fe(II) catalyzed dissolution. However, these reactions lead to the same overall dissolution reaction as R4a. The reactions and the previously determined rate coefficients are described in more detail in our previous papers (Biswakarma et al., 2019; Kang et al., 2019; Biswakarma et al., 2020). Although Fe(II)-catalyzed dissolution is facilitated by the presence of Fe(II), it is a net non-reductive ligand-controlled dissolution, forming dissolved Fe(III) complexes (R4a-R4c). New Fe(II) surface sites are continuously formed from the bulk solid (R2h and R4d). For reactions R1a-c, R4a-d, and for reaction R5 describing the formation of Fe(II) complexes in solution, we used the rate coefficients as determined under the same conditions for DFOB in our previous study (Biswakarma et al., 2020), and adapted rate coefficients from the previous study with EDTA (Biswakarma et al., 2019). Reactions 6a and 6b describe the oxidation of surface Fe(II) by H_2O_2 and by dissolved O_2. The reaction rates for these reactions were adjusted, as described in the footnotes of Table 2. The model as entered in Acuchem, and the complete list of rate coefficients used for the fits are provided in Tables S3a and S3b.

4.1.2. Photoinduced formation of Fe(II)

Light absorption in the bulk of Lp or Gt leads to formation of electron-hole pairs (R2a) and to charge migration and trapping of charges on the surface (R2b) (Borer et al., 2009c), summarized in R2ab. Fast charge recombination in the bulk and on the surface (R2c) leads to low yields of Fe(II) and Fe(IV) or $^{\bullet}OH$-radicals (R2d) and H_2O_2 (R2e) in the absence of ligands. Adsorbed ligands, however,

can act as efficient hole scavengers on the surface (R2f) and increase the production Fe(II) by preventing charge recombination between Fe(II) and Fe(IV) surface sites (R2c). In the presence of ligands forming photoreactive surface complexes, Fe(II) can also be produced by absorption of light by surface complexes (R2g). EDTA and DFOB can thus promote formation of Fe(II) both by scavenging Fe(IV) on the surface and thus preventing charge recombination, and by acting as chromophores with production of Fe(II) in LMCT transitions. In addition, surface hydroxyl groups can also act as chromophores and produce Fe(II) and $^{\bullet}OH$ on the surface in LMCT transitions (not shown in the Table 2), but yields are lower due to fast back reactions between $^{\bullet}OH$ and Fe(II) formed at the same site. When EDTA acts a scavenger of surface Fe(IV) (R9a), reaction products of the ligand can reduce a second surface Fe(III) to Fe(II) (R9b). Reaction R9b or reaction R9c under oxic conditions can form stable products (e.g. ethylenediaminetriacetate (ED3A) (Karametaxas et al., 1995) and oxidants such as $^{\bullet}O_2^-$ (R7c, R9c) and H_2O_2 (R7d).

To identify the most relevant reaction pathways, rates of light absorption were calculated with the emission spectrum of the light source and the absorbance spectra of Lp, Gt, EDTA and DFOB (Fig. S1) and compared to the rates of Fe(II) formation and dissolution (Tables 1a and 1b). With concentrations of dissolved Fe(III)-ligand complexes below 5 µM at the first illumination, over 99.7 % of the light between 320 nm and 450 nm was absorbed by Gt and Lp. The maximum rates of photochemical formation of Fe(II) with 5 µM dissolved Fe(III)EDTA, calculated with the quantum yield of 0.031 at 365 nm (Kari et al., 1995), are listed in Table 1a. Also listed are calculated rates of Fe(II) production from absorption of light by 10 µM EDTA surface complexes, assuming that the quantum yields are the same as for the solution complexes. Corresponding rates for DFOB are not listed, as the quantum yields for Fe(II) formation from adsorbed DFOB are much smaller than for EDTA according to ATR-FTIR measurements (Borer et al., 2005; Borer et al., 2009b). As mentioned above, rates of Fe(II) formation were measured by complexation of the formed Fe(II) with phen.

The measured rate of photochemical Fe(II) formation with EDTA was by a factor of 4-5 larger than the estimated combined rate of Fe(II) production from 5 µM Fe(III)EDTA solution and 10 µM surface complexes. This indicates that either the surface complexes photochemically produced Fe(II) (R7a, R10a) with a much higher quantum yield than the corresponding complexes in solution, or that bulk Lp and Gt are the chromophore (effective absorber of light) and surface complexes act as scavengers

for surface Fe(IV) (R2f, R9a). Scavenging of surface Fe(IV) is the more likely mechanism, as 2-3 times higher rates of photochemical Fe(II) formation were also observed with DFOB, which, due its low photoreactivity, is expected to act predominantly as a hole scavenger. The finding that light absorption by solids is more important than light absorption by surface complexes agrees with previous studies (Borer et al., 2005) that found that Fe(II) is produced predominantly by the intrinsic photoactivity of Lp. However, the same authors also found evidence for photoreactivity of adsorbed DFOB in a later study of wavelength-dependent dissolution of Lp (Borer et al., 2009d). For both processes, the role of DFOB in photoreductive dissolution was ascribed to DFOB facilitating the release of photogenerated Fe(II) from the surface during illumination (Borer et al., 2005; Borer et al., 2009b; Borer et al., 2009d). In this study, we found that photo-generated Fe(II) also accelerates the release of Fe(III), even after illumination stops. In the absence of ligands, charge recombination results in low yields of Fe(II), $^{\bullet}OH$ and H_2O_2, as reported previously for Lp (Borer et al., 2009c). The about 12 times larger Fe(II) production by Lp compared to Gt in the absence of ligands indicates that charge recombination is more efficient in Gt than in Lp. In the presence of EDTA, the yields of Fe(II) from Lp and Gt are similar and larger than in the presence of DFOB, which shows that charge migrates to the surface and that adsorbed EDTA is a more efficient hole scavenger in both Lp and Gt than DFOB. The relative enhancement of the photoproduction of Fe(II) in Lp and Gt by DFOB (by factors of 2-3) are similar, but in Lp the absolute increase of Fe(II) production by DFOB is much larger than for Gt. An explanation for these differing effects is beyond the scope and was not the subject of this study. However, important in the context of Fe(II) catalyzed ligand-controlled dissolution is that (1) >99% of the incident light was adsorbed in the bulk of Lp and Gt at the start of the reactions, and (2) photochemical charge separation in the bulk and migration of charge to surface appears to be the dominant pathway for the formation of Fe(II). In our kinetic model, we accounted for the different yields of Fe(II) (R2ab) in the presence of EDTA and DFOB by entering reaction coefficients determined from the rates of photochemical formation of Fe(II) listed in Table 1a.

The rate coefficients for photochemical Fe(II) production calculated from the rates listed in Table 1, together with the previously determined rate coefficients for non-catalyzed and catalyzed dissolution for EDTA (Biswakarma et al., 2019) and for DFOB (Biswakarma et al., 2020) resulted in acceptable fits of the data shown in Figures 2 and 3. The rate coefficients for EDTA were adjusted, as previously

determined rate coefficients were for pH 6.0 and for slightly different expressions describing the first steps of Fe(II) catalyzed dissolution. For the fits shown for DFOB in Figure 3, we adjusted only rate coefficients for the oxidation of adsorbed Fe(II) and for the formation of H_2O_2 on the surface.

4.1.3. Catalytic effect induced by illumination

Similar to the catalytic effect (CE) described in our previous studies, we define a photocatalytic effect (CE_p) as $CE_p = R_{Fe,diss,,p} / R_{Fe,diss}$ where $R_{Fe,diss}$ is the rate of dissolution in the dark without illumination, and $R_{Fe,diss,,p}$ is the rate of dissolution after or during illumination (as listed in Table 1b). Under anoxic conditions, values for the observed CE_p with 2.15 µM photogenerated Fe(II) on the dissolution of Lp with EDTA were 33 at pH 6.0 and 8 at pH 7.0. For Lp and DFOB, CE_p was 7-10 for DFOB at pH 7.0. This compares to a CE of 22 for EDTA at pH 6.0 and a CE of 26 for DFOB at pH 7.0 after addition of 2 µM Fe(II) in our previous studies (Table S2). With Gt and EDTA, the CE_p of 28-42 with 2.7 µM photoproduced Fe(II) compares well to the CE of 7.9 and 13 with 1.0 µM added HBED measured in our previous study (assuming effected proportional to Fe(II) concentrations) (Kang et al., 2019). The seemingly lower effect of Fe(II) with DFOB at pH 7.0 can be explained by oxidation of a fraction of the photoproduced Fe(II) by reactive oxidants ($^{\bullet}OH$, $^{\bullet}O_2^-$ and H_2O_2).

4.1.4. Steady-state concentrations of Fe(II) in oxic systems

Under oxic conditions, a lasting effect of photoproduced Fe(II) on the dissolution rate after intermittent illumination was not observed with the time resolution of minutes in our experiments. However, during continuous illumination, the dissolution of Lp was still accelerated by factors of 4.8 with EDTA and by 5.5 with DFOB at pH 7.0. Steady state concentrations of adsorbed Fe(II) under oxic conditions can be estimated with the rates of photochemical formation of Fe(II) (R_{phot}) and rates of oxidation of adsorbed Fe(II) with dissolved O_2, with the expression $[\equiv Fe(II)]_{ss} = R_{phot}/k_{ox}$. Reported values for k_{ox} for heterogeneous oxidation of Fe(II) with various Fe(III)(hydr)oxides at pH 6-7 and 250 µM dissolved O_2 range from 1×10^{-3} - 1×10^{-2} s^{-1}.(Barnes et al., 2009) Kinsela et al. determined a rate-coefficient for oxidation of Fe(II) adsorbed to Lp at pH 7.0 of 88.7 $M^{-1}s^{-1}$, corresponding to k_{ox} $=2.2\times10^{-2}$ s^{-1} with 250 µM dissolved O_2 (Kinsela et al., 2016). Similar rates for the oxidation of Fe(II) adsorbed to Lp were recently found in our related detailed study on the rates of oxidation of Fe(II) in

the presence of various Fe(III) (hydr)oxide minerals (Kang, 2019). The calculated $[\equiv Fe(II)]_{ss}$ listed in Table 1a show that $[\equiv Fe(II)]_{ss}$ during continuous illumination under oxic conditions are by factors of ~~10~~5-20 lower than concentrations of Fe(II) produced from 5-15 min intermittent illuminations under anoxic conditions.

The smaller catalytic effects under oxic conditions are thus consistent with the smaller (steady state) concentrations of Fe(II), considering that additional oxidation of adsorbed Fe(II) by $^{\bullet}OH$, O_2^- and H_2O_2 might further reduce concentrations Fe(II). For Gt, a catalytic effect could only be observed with EDTA under anoxic conditions. The catalytic effect on the dissolution of Gt under oxic conditions was too small to be observed on the time scale of hours, in agreement with previous results.

The rate coefficient for the oxidation of adsorbed Fe on the surface Lp by dissolved oxygen found in the kinetic model (R6b) falls within the range of $1 \cdot 10^{-3}$ - $1 \cdot 10^{-2}$ s^{-1}, in agreement with the range found previously (Barnes et al., 2009; Kinsela et al., 2016). Concentrations of Fe(II) and H_2O_2, formed during intermittent illuminations of Lp in the presence of DFOB, as calculated with the kinetic model, are shown in Figure S12. The modeled concentrations of Fe(II) are in reasonable agreement with the concentrations listed in Table 1a. The modeled concentrations of H_2O_2 are in the range of previously measured H_2O_2 concentrations in illuminated suspension of Lp in the absence of DFOB and EDTA (Borer et al., 2009c).

4.1.5. Photoreductive dissolution and Fe(II)-catalyzed ligand-controlled dissolution

The combined results of anoxic and oxic experiments with intermittent illumination provide novel insights about the mechanisms of photochemically promoted dissolution of Fe(III)(hydr)oxides. So far the rate of photochemical Fe(II) formation has been assumed to be limiting factor for photoinduced dissolution. Here, we show that photochemically formed Fe(II) plays an important additional role by catalyzing non-reductive dissolution as an additional pathway. Under anoxic conditions and with short illuminations, this pathway was dominant in our experiments. Even short illuminations lead to continued accelerated, net non-reductive dissolution. Under oxic conditions, both Fe(II)-catalyzed and photoreductive dissolution contribute, but cannot easily be distinguished, because adsorbed and dissolved Fe(II)EDTA and Fe(II)DFOB complexes are oxidized by both charge transfer to the surface and by dissolved O_2.

4.1.6. Photoreactivity of dissolved complexes

With continuous illumination, ligands in dissolved photolabile Fe(III)-complexes, such as Fe(III)EDTA, are photodegraded (R7a and R12a). Several subsequent reactions can lead to further degradation of the ligands (R7b-f). In addition, reactions of ligands with surface-bound hydroxyl radical can also contribute (R8b). The initially formed radicals ($^{\bullet}$L in R7a) are oxidized to stable products (P in R7c) that are no longer able to maintain Fe(III) in solution at pH 7.0 and above. Ethylenediamine-N,N'-triacetic acid (ED3A), is the first product resulting from decarboxylation and subsequent oxidation of EDTA (R12a-b) (Karametaxas et al., 1995; Kocot et al., 2006). Subsequent decarboxylation steps result in ethylenediamine-N,N'-diacetic acid (ED2A) and further degradation products which are not able to prevent formation and precipitation of Fe(III)(hydr)oxides. In contrast, dissolved Fe(III)DFOB complexes are much less susceptible to photodegradation. Some limited degradation of adsorbed DFOB from oxidation by $^{\bullet}$OH or Fe(IV) or by light absorption and LMCT transitions in surface complexes must have occurred to explain the higher yields of Fe(II) in the presence of DFOB compared to its absence. Borer et al. (2009) reported that in Lp suspensions at pH 8.0, absorption of light from 395-435 nm by surface complexes of DFOB contributed to formation of Fe(II) by photoinduced LMCT (Borer et al., 2009d). In our experiments, less than 30% of the DFOB was degraded after 7 h of illumination, based on 35 µM dissolved Fe(III)DFOB (as determined by UV spectroscopy). The ability of the ligand to form photostable complexes is important to keep Fe in solution. Barbeau et al. (Barbeau et al., 2003) studied the photoreactivity of dissolved Fe(III)-ligand complexes of marine siderophores in relation to their Fe(III)-complexing functional groups and found that: (a) hydroxamate groups were photochemically resistant regardless of Fe(III) complexation, (b) α-hydroxycarboxylates were photostable when uncomplexed, but photoreactive when complexed, and (c) catecholates were photoreactive when uncomplexed but photostable when complexed. High photoreactivities of carboxylates and α-hydroxycarboxylates were also observed with in-situ ATR-FTIR when complexed to the surfaces of various iron(hydr)oxides (Borer et al., 2007; Borowski et al., 2018). Low or no photoreactivity of DFOB on the surface of Lp was detected with ATR-FTIR (Borer et al., 2009a; Borer et al., 2009b). However, some of the same authors found evidence for some photoreactivity of DFOB adsorbed to Lp in experiments assessing the wavelength dependency of

photoinduced dissolution at pH 8.0 (Borer et al., 2009d) Although quantum yields for Fe(II) formation and degradation of adsorbed DFOB were not measured, they are lower than for EDTA based on ATR-FTIR measurements (Borer et al., 2009a; Biswakarma et al., 2019). DFOB is thus degraded only slowly during continuous illumination, in contrast to EDTA, which is degraded quickly in solution and on the surface of Lp as discussed above. This study shows that the photostability of ligands is a crucial factor in the photochemical mobilization of Fe(II) and Fe(III). Many siderophores (e.g. aerobactin and pyoverdin) have one or several carboxyl groups and could potentially produce Fe(II) efficiently while retaining their ability to complex Fe(II) after decarboxylation (Borer et al., 2009c; Passananti et al., 2016). The kinetic model was able to model the continuous illumination experiments (Figure 4) under oxic conditions with limited degradation of DFOB and the complete degradation of EDTA reasonably well.

4.1.7. Limitations of the kinetic model

The kinetic modeling shows that the experimental observations can be explained by the list of reactions listed in Table 2a. However, it is important to point out that good fits do not prove that the list of reactions is correct and complete. Alternative models might explain the data equally well. We did not attempt to find unique rate coefficients for each reaction. The reason for this is that many of the rate coefficients are interdependent and it is not possible to determine them without additional experiments and data. Our aim was to explain the data with the previously determined rate coefficients for Fe(II)-catalyzed dissolution and a minimal number of additional reactions and rate coefficients within expected and physically reasonable ranges (see footnotes of Table 2). Without being able to fit all data points perfectly well, the model reproduces the data sufficiently well to support the suggested reactions. We did not fit the data at pH 6.0 and pH 8.5 because the datasets at these pH-values are not as complete as the data sets at pH 7.0.

4.2. Environmental Implications

Fe(III)(hydr)oxides are ubiquitous on soil-water interfaces and as suspended particles in the water column of aquatic environments that are exposed to sunlight. Understanding the role of photoreactions in the dissolution pathways of Fe(III)(hydr)oxides in redox dynamic environments is an important step

to better comprehend the cycles of Fe and other (trace) elements in natural environments. The findings of this study, show that Fe(II) produced upon 5-15 min exposure of Lp- or Gt-suspensions to light can act as a catalyst for continued accelerated ligand-controlled dissolution, may allow us to predict the bioavailability of iron and the mobility of associated trace elements in different environments.

Under anoxic conditions, periods of 5-15 min illumination accelerate the dissolution of Fe(III)(hydr)oxides (as shown in this study for both Lp and Gt) by factors up to 40, even after illumination stops. Anoxic environments that can be reached by sunlight exist in shallow lakes (Oswald et al., 2015), ponds (Finlay et al., 1996), and reservoirs (Townsend, 1999; Hamre et al., 2018). Cyanobacterial blooms are often considered to be an indicator for the quality of the water (Hrudey et al., 2006; Merel et al., 2013; de Paul Obade and Moore, 2018). Light-induced dissolution of Fe phases could play an important role in algal blooms, where rapid growth of cyanobacteria can be limited by bio-accessible iron (Zhang et al., 2017). Sub-oxic and anoxic micro-environments caused by microbial reduction were found in overall oxic water in cyanobacterial aggregates in surface blooms (Ploug, 2008) or in settling fecal pellets and aggregates (Shaked and Lis, 2012). Concentrations of ligands with reactive hydroxamate moieties were positively correlated to cyanobacterial biomass in lakes with low Fe bioavailability (Sorichetti et al., 2016). Although anoxic sunlit conditions represent the far end of environmentally-relevant conditions, the presented results are relevant for a better understanding of dissolution reactions and of the release of nutrients and contaminants and their uptake by biota in suboxic and oxic environments.

Under oxic conditions, photo-stable ligands are required to sustain higher concentrations of dissolved Fe under sunlit conditions. EDTA and, most likely, similar ligands with photoactive carboxylate groups can accelerate dissolution, but are photodegraded rapidly. Ligands such as DFOB with hydroxamate groups are more photostable and are able to keep Fe in solution. Many natural siderophores contain carboxylate and hydroxamate groups and preserve their ability to complex Fe(III) after decarboxylation. In natural environments, ranges of ligands are present and may have different functions in the mobilization and bioavailability of Fe. The acceleration of dissolution processes by photochemically formed Fe(II) are highly dependent on the structure of the Fe phase, the functional groups of the ligand, and the oxygen concentrations. This study shows that parallel and in addition to

photo reductive dissolution, Fe(II)-catalyzed dissolution can be an important pathway for Fe(III) mobilization in sunlit waters.

5. Conclusions

Illumination of circumneutral, carbonate buffered suspensions of Gt and Lp lead to accelerated dissolution in the presence of EDTA and DFOB. Dissolution rates were not only accelerated by photoreduction of surface Fe(III) and facilitated detachment of Fe(II) by the ligands (as previously described), but also by Fe(II)-catalyzed detachment of Fe(III)-ligand complexes that can continue after illumination stops. Kinetic modeling confirmed that the suggested reactions are able to explain the experimentally-measured data. Under anoxic conditions, short (5-15 min) illuminations lead to up to 40 times accelerated dissolution rates during subsequent dark periods. Under oxic conditions, Fe(II) on the surface was oxidized within seconds to minutes by dissolved O_2, which prevented a continued catalytic action of Fe(II) after illumination stopped. Continuous illumination under oxic conditions lead to steady state concentrations of Fe(II) that still accelerated dissolution rates by factors of 3-5. In addition to the catalytic effect of photogenerated Fe(II), this study shows that the photostability of dissolved Fe(III)-ligand complexes is crucial for the mobilization of iron by light under oxic conditions. While EDTA lead to high initial yields of Fe(II) due to the high photoreactivity of surface and of dissolved Fe(III)EDTA complexes, EDTA was photodegraded and the products were not able to hold Fe(III) in solution during continuous illumination at circumneutral pH. In contrast, DFOB formed photostable dissolved complexes which were able to maintain Fe(III) in solution over several hours of illumination. These results show that the catalytic effect of Fe(II) on ligand-controlled dissolution and the different stabilities of Fe(III)complexes are important factors in the mobilization and bioavailability of iron. The findings likely apply to a wide range of sunlit aqueous environments.

CRediT authorship contribution statement

Jagannath Biswakarma: Conceptualization, Methodology, Investigation, Writing - original draft. **Kyounglim Kang:** Conceptualization, Investigation, Contribution to final document. **Walter D.C. Schenkeveld:** Conceptualization, Review & editing, Funding acquisition. **Stephan M. Kraemer:**

Conceptualization, Review & editing, Funding acquisition. **Janet G. Hering:** Conceptualization, Supervision, Review & editing, Funding acquisition. **Stephan J. Hug:** Conceptualization, Methodology, Supervision, Writing - review & editing, Funding acquisition, Project administration.

Declaration of Competing Interest

The authors declare that they have no known competing financial interests or personal relationships that could have appeared to influence the work reported in this paper.

Acknowledgements

The authors are grateful to Thomas Rüttimann (Eawag) for laboratory experiments and technical assistance. This project was financially supported by the Swiss National Science Foundation, project number 200021L_150150 ‘‘Synergistic effects of redox processes and ligand controlled dissolution of iron(hydr)oxide phases” Mathematics, Natural sciences and Engineering (division II). SK, WS and KK were supported by the Austrian Science Fund (FWF, Grant No.: I 1528-N19 and I 2865-N34, respectively).

Appendix A. Supplementary material

Supplementary data to this article can be found online.

References

AlSalka, Y., Granone, L.I., Ramadan, W., Hakki, A., Dillert, R., Bahnemann, D.W., 2019. Iron-based photocatalytic and photoelectrocatalytic nano-structures: Facts, perspectives, and expectations. Applied Catalysis B: Environmental 244, 1065-1095.

Barbeau, K., Rue, E.L., Trick, C.G., Bruland, K.T., Butler, A., 2003. Photochemical reactivity of siderophores produced by marine heterotrophic bacteria and cyanobacteria based on characteristic Fe(III) binding groups. Limnology and Oceanography 48, 1069-1078.

Barnes, A., Sapsford, D.J., Dey, M., Williams, K.P., 2009. Heterogeneous Fe(II) oxidation and zeta potential. Journal of Geochemical Exploration 100, 192-198.

Biswakarma, J., Kang, K., Borowski, S.C., Schenkeveld, W.D.C., Kraemer, S.M., Hering, J.G., Hug, S.J., 2019. Fe(II)-Catalyzed Ligand-Controlled Dissolution of Iron(hydr)oxides. Environmental Science & Technology 53, 88-97.

Biswakarma, J., Kang, K., Schenkeveld, W.D.C., Kraemer, S.M., Hering, J.G., Hug, S.J., 2020. Linking Isotope-Exchange with Fe(II)-Catalyzed Dissolution of Iron (hydr)oxides in the Presence of Bacterial Siderophore Deferoxamine-B Environmental Science & Technology 54, 768-777.

Borer, P., Hug, S.J., 2014. Photo-redox reactions of dicarboxylates and α-hydroxydicarboxylates at the
Interface Science 416, 44-53.
Borer, P., Hug, S.J., Sulzberger, B., Kraemer, S.M., Kretzschmar, R., 2007. Photolysis of citrate on the surface of lepidocrocite: An in situ attenuated total reflection infrared spectroscopy study. Journal of Physical Chemistry C 111, 10560-10569.
Borer, P., Hug, S.J., Sulzberger, B., Kraemer, S.M., Kretzschmar, R., 2009a. ATR-FTIR spectroscopic study of the adsorption of desferrioxamine B and aerobactin to the surface of lepidocrocite (gamma-FeOOH). Geochimica Et Cosmochimica Acta 73, 4661-4672.
Borer, P., Kraemer, S.M., Sulzberger, B., Hug, S.J., Kretzschmar, R., 2009b. Photodissolution of lepidocrocite (gamma-FeOOH) in the presence of desferrioxamine B and aerobactin. Geochimica Et Cosmochimica Acta 73, 4673-4687.
Borer, P., Sulzberger, B., Hug, S.J., Kraemer, S.M., Kretzschmar, R., 2009c. Photoreductive Dissolution of Iron(III) (Hydr)oxides in the Absence and Presence of Organic ligands: Experimental Studies and Kinetic Modeling. Environmental Science & Technology 43, 1864-1870.
Borer, P., Sulzberger, B., Hug, S.J., Kraemer, S.M., Kretzschmar, R., 2009d. Wavelength-Dependence of Photoreductive Dissolution of Lepidocrocite (gamma-FeOOH) in the Absence and Presence of the Siderophore DFOB. Environmental Science & Technology 43, 1871-1876.
Borer, P.M., Sulzberger, B., Reichard, P., Kraemer, S.M., 2005. Effect of siderophores on the light-induced dissolution of colloidal iron(III) (hydr)oxides. Marine Chemistry 93, 179-193.
Borowski, S.C., Biswakarma, J., Kang, K., Schenkeveld, W.D.C., Hering, J.G., Kubicki, J.D., Kraemer, S.M., Hug, S.J., 2018. Structure and reactivity of oxalate surface complexes on lepidocrocite derived from infrared spectroscopy, DFT-calculations, adsorption, dissolution and photochemical experiments. Geochimica Et Cosmochimica Acta 226, 244-262.
Braun, W., Herron, J.T., Kahaner, D.K., 1988. Acuchem: A computer program for modeling complex chemical reaction systems. Int J Chem Kinet 20, 51-62.
de Paul Obade, V., Moore, R., 2018. Synthesizing water quality indicators from standardized geospatial information to remedy water security challenges: A review. Environment International 119, 220-231.
Faust, B.C., Hoigne, J., 1990. Photolysis of Fe(III)-Hydroxy Complexes as Sources of Oh Radicals in Clouds, Fog and Rain. Atmospheric Environment Part a-General Topics 24, 79-89.
Faust, B.C., Zepp, R.G., 1993. Photochemistry of Aqueous Iron(III) Polycarboxylate Complexes - Roles in the Chemistry of Atmospheric and Surface Waters. Environmental Science & Technology 27, 2517-2522.
Finlay, B.J., Maberly, S.C., Esteban, G.F., 1996. Spectacular abundance of ciliates in anoxic pond water: Contribution of symbiont photosynthesis to host respiratory oxygen requirements. Fems Microbiology Ecology 20, 229-235.
Fu, H.B., Cwiertny, D.M., Carmichael, G.R., Scherer, M.M., Grassian, V.H., 2010. Photoreductive dissolution of Fe-containing mineral dust particles in acidic media. Journal of Geophysical Research-Atmospheres 115.
Goldberg, M.C., Cunningham, K.M., Weiner, E.R., 1993. Aquatic Photolysis - Photolytic Redox Reactions between Goethite and Adsorbed Organic-Acids in Aqueous-Solutions. Journal of Photochemistry and Photobiology a-Chemistry 73, 105-120.
Hamre, K.D., Lofton, M.E., McClure, R.P., Munger, Z.W., Doubek, J.P., Gerling, A.B., Schreiber, M.E., Carey, C.C., 2018. In situ fluorometry reveals a persistent, perennial hypolimnetic cyanobacterial bloom in a seasonally anoxic reservoir. Freshwater Science 37, 483-495.
Hatchard, C.G., Parker, C.A., 1956. A New Sensitive Chemical Actinometer .2. Potassium Ferrioxalate as a Standard Chemical Actinometer. Proceedings of the Royal Society of London Series a-Mathematical and Physical Sciences 235, 518-536.
Hrudey, S.E., Hrudey, E.J., Pollard, S.J.T., 2006. Risk management for assuring safe drinking water. Environment International 32, 948-957.
Hug, S.J., Canonica, L., Wegelin, M., Gechter, D., Von Gunten, U., 2001. Solar oxidation and removal of arsenic at circumneutral pH in iron containing waters. Environmental Science & Technology 35, 2114-2121.
Johnson, K.S., Coale, K.H., Elrod, V.A., Tindale, N.W., 1994. Iron Photochemistry in Seawater from the Equatorial Pacific. Marine Chemistry 46, 319-334.
Kang, K., 2019. Catalytic effects of Fe(II) on ligand-controlled dissolution of Fe(III) (hydr)oxide phases. University of Vienna, Vienna, p. 187.

Kang, K., Schenkeveld, W.D.C., Biswakarma, J., Borowski, S.C., Hug, S.J., Hering, J.G., Kraemer,

Minerals in the Presence of Diverse Ligands and over a Broad pH Range. Environmental Science & Technology 53, 98-107.
Karametaxas, G., Hug, S.J., Sulzberger, B., 1995. Photodegradation of EDTA in the Presence of Lepidocrocite. Environmental Science & Technology 29, 2992-3000.
Kari, F.G., Hilger, S., Canonica, S., 1995. Determination of the Reaction Quantum Yield for the Photochemical Degradation of Fe(III)-EDTA- Implications for the Environmental Fate of EDTA in Surface Waters. Environmental Science & Technology 29, 1008-1017.
Kim, D., Duckworth, O.W., Strathmann, T.J., 2009. Hydroxamate siderophore-promoted reactions between iron(II) and nitroaromatic groundwater contaminants. Geochimica Et Cosmochimica Acta 73, 1297-1311.
Kim, D., Duckworth, O.W., Strathmann, T.J., 2010a. Reactions of aqueous iron-DFOB (desferrioxamine B) complexes with flavin mononucleotide in the absence of strong iron(II) chelators. Geochimica Et Cosmochimica Acta 74, 1513-1529.
Kim, K., Choi, W., Hoffmann, M.R., Yoon, H.I., Park, B.K., 2010b. Photoreductive Dissolution of Iron Oxides Trapped in Ice and Its Environmental Implications. Environmental Science & Technology 44, 4142-4148.
Kinsela, A.S., Jones, A.M., Bligh, M.W., Pham, A.N., Collins, R.N., Harrison, J.J., Wilsher, K.L., Payne, T.E., Waite, T.D., 2016. Influence of Dissolved Silicate on Rates of Fe(II) Oxidation. Environmental Science and Technology 50, 11663-11671.
Kocot, P., Karocki, A., Stasicka, Z., 2006. Photochemistry of the Fe(III)-EDTA complexes - A mechanistic study. Journal of Photochemistry and Photobiology a-Chemistry 179, 176-183.
Kraemer, S.M., Butler, A., Borer, P., Cervini-Silva, J., 2005. Siderophores and the dissolution of iron-bearing minerals in marine systems. Reviews in Mineralogy and Geochemistry, pp. 53-84.
Kuma, K., Nakabayashi, S., Matsunaga, K., 1995. Photoreduction of Fe(III) by Hydroxycarboxylic Acids in Seawater. Water Research 29, 1559-1569.
Kunkely, H., Vogler, A., 2001. Photoreduction of aqueous ferrioxamine B by oxalate induced by outer-sphere charge transfer excitation. Inorganic Chemistry Communications 4, 215-217.
Litter, M.I., Baumgartner, E.C., Urrutla, G.A., Blesa, M.A., 1991. Photodissolution of Iron Oxides. 3. Interplay of Photochemical and Thermal Processes in Maghemite/Carboxylic Acid Systems. Environmental Science and Technology 25, 1907-1913.
Litter, M.I., Blesa, M.A., 1988. Photodissolution of iron oxides. I. Maghemite in EDTA solutions. Journal of Colloid And Interface Science 125, 679-687.
Merel, S., Walker, D., Chicana, R., Snyder, S., Baurès, E., Thomas, O., 2013. State of knowledge and concerns on cyanobacterial blooms and cyanotoxins. Environment International 59, 303-327.
Oswald, K., Milucka, J., Brand, A., Littmann, S., Wehrli, B., Kuypers, M.M.M., Schubert, C.J., 2015. Light-Dependent Aerobic Methane Oxidation Reduces Methane Emissions from Seasonally Stratified Lakes. Plos One 10.
Passananti, M., Vinatier, V., Delort, A.M., Mailhot, G., Brigante, M., 2016. Siderophores in Cloud Waters and Potential Impact on Atmospheric Chemistry: Photoreactivity of Iron Complexes under Sun-Simulated Conditions. Environmental Science & Technology 50, 9324-9332.
Pehkonen, S.O., Siefert, R., Erel, Y., Webb, S., Hoffmann, M.R., 1993. Photoreduction of Iron Oxyhydroxides in the Presence of Important Atmospheric Organic-Compounds. Environmental Science & Technology 27, 2056-2062.
Ploug, H., 2008. Cyanobacterial surface blooms formed by Aphanizomenon sp and Nodularia spumigena in the Baltic Sea: Small-scale fluxes, pH, and oxygen microenvironments. Limnology and Oceanography 53, 914-921.
Rijkenberg, M.J.A., Gerringa, L.J.A., Carolus, V.E., Velzeboer, I., de Baar, H.J.W., 2006. Enhancement and inhibition of iron photoreduction by individual ligands in open ocean seawater. Geochimica Et Cosmochimica Acta 70, 2790-2805.
Shaked, Y., Lis, H., 2012. Disassembling Iron Availability to Phytoplankton. Frontiers in Microbiology 3.
Sherman, D.M., 2005. Electronic structures of iron(III) and manganese(IV) (hydr)oxide minerals: Thermodynamics of photochemical reductive dissolution in aquatic environments. Geochimica Et Cosmochimica Acta 69, 3249-3255.
Sorichetti, R.J., Creed, I.F., Trick, C.G., 2016. Iron and iron-binding ligands as cofactors that limit cyanobacterial biomass across a lake trophic gradient. Freshwater Biology 61, 146-157.

Sulzberger, B., Laubscher, H., 1995a. Photochemical Reductive Dissolution of Lepidocrocite - Effect Interspecies Processes. Amer Chemical Soc, Washington, pp. 279-290.
Sulzberger, B., Laubscher, H., 1995b. Reactivity of Various Types of Iron(III) (Hydr)Oxides Towards Light-Induced Dissolution. Marine Chemistry 50, 103-115.
Townsend, S.A., 1999. The seasonal pattern of dissolved oxygen, and hypolimnetic deoxygenation, in two tropical Australian reservoirs. Lakes & Reservoirs: Science, Policy and Management for Sustainable Use 4, 41-53.
Voelker, B.M., Morel, F.M.M., Sulzberger, B., 1997. Iron redox cycling in surface waters: Effects of humic substances and light. Environmental Science & Technology 31, 1004-1011.
von der Heyden, B.P., Roychoudhury, A.N., Mtshali, T.N., Tyliszczak, T., Myneni, S.C.B., 2012. Chemically and Geographically Distinct Solid-Phase Iron Pools in the Southern Ocean. Science 338, 1199-1201.
Waite, T.D., 1990. Photo-Redox Processes at the Mineral-Water Interface. Reviews in Mineralogy 23, 559-603.
Waite, T.D., Morel, F.M.M., 1984. Photoreductive Dissolution of Colloidal Iron Oxides in Natural Waters. Environmental Science & Technology 18, 860-868.
Wells, M.L., Mayer, L.M., Donard, O.F.X., Sierra, M.M.D., Ackelson, S.G., 1991. The Photolysis of Colloidal Iron in the Oceans. Nature 353, 248-250.
Zhang, T., He, J., Luo, X., 2017. Effect of Fe and EDTA on Freshwater Cyanobacteria Bloom Formation. Water 9, 326.

Tables and Figures

Table 1a. Photochemical formation of Fe(II) measured with phen (anoxic), quantum yields for Fe(II) formation, and calculated steady state concentrations of Fe(II) under oxic conditions: ($[Fe(II)]_{ss\ (oxic)}$)

Rate of photon absorption in Lp and Gt suspensions during illumination: 1,038,000 (nM/min)							
		Illum. Time (min)	[Fe(II)] (µM)	d[FeII)]/dt (nM/min)	*d[FeII)]/dt** *(nM/min)*	Quantum yield ΦFe(II)	$[Fe(II)]_{ss}$ (oxic)
Lp	EDTA	5	2.15	430	*32 / 64*	6.2×10^{-4}	0.48
Lp	DFOB	15	2.70	180	-	1.9×10^{-4}	0.15
Gt	EDTA	5	2.70	540	*43 / 86*	5.2×10^{-4}	0.41
Gt	DFOB	15	0.15	10	-	-	0.01
Lp	none	15	1.20	79	-	7.7×10^{-5}	0.06
Gt	none	15	0.10	6	-	-	0.00

* *Calculated rate of Fe(II) formation from 5 µM Fe(III)L / 10 µM ≡Fe(III)*

Table 1b. Dissolution rates ($d[Fe]_{diss}/dt$) of Lp and Gt with 50 µM ligand at pH 7.0 in the dark and under illumination, and catalytic effect (CE_p). Rates at pH 6.0 and 8.5 are reported in *italic* font.

		Illum. Time (min)	[Fe(II)] (µM)	$d[Fe]_{diss}/dt$ (nM/min)		CE_p	CE_p	$d[Fe]_{diss}/dt$ (% h^{-1})	
				anoxic	oxic	anoxic	oxic	anoxic	oxic
$[Fe]_{diss}$ formation in the dark									
Lp	EDTA	-	-	31	25	-	-	0.17	0.13
Lp	DFOB	-	-	19	19	-	-	0.10	0.10
Gt	EDTA	-	-	1.3	-	-		0.01	-
Gt	DFOB	-	-	-	-			-	-
$[Fe]_{diss}$ formation during continuous UV-A									
Lp	EDTA			831	121	27	4.8	4.43	0.65
	DFOB			312	105	16	5.5	1.66	0.56
$[Fe]_{diss}$ formation after intermittent UV-A									
Lp	EDTA	5	2.15	238	-	8	-	1.27	-
	EDTA	5	2.15	-	-		-	-	-
	EDTA	5	2.15	-	-		-	-	-
	EDTA	15	6.45	427	-	14	-	2.28	-
Lp	DFOB	15	2.70	173	-	9	-	0.92	-
	DFOB	15	2.70	198	-	10	-	1.06	-
	DFOB	15	2.70	131	-	7	-	0.70	-
Gt	EDTA	5	2.70	51	-	39	-	0.27	-
	EDTA	5	2.70	55	-	42	-	0.29	-
	EDTA	5	2.70	37	-	28	-	0.20	-
pH 6.0, Lp/ EDTA in the dark				*26*	*26*	-	-	*0.14*	*0.14*
Lp/ EDTA after 5 min intermittent UV-A				*859*	-	*33*	-	*4.58*	
pH 8.5									
Lp	*DFOB*	*none (i.e. dark)*		*39*	*30*			*0.21*	*0.16*
Lp	*DFOB*	*15*		*84*		*2*		*0.45*	
	DFOB	*15*		*88*		*2*		*0.47*	
	DFOB	*15*		*79*		*2*		*0.42*	

Table 2a. List of reactions used for kinetic modeling

Reaction				k or K (s^{-1}, $M^{-1}s^{-1}$, M^{-1})	
				(EDTA / DFOB)	
Non-catalyzed dissolution					
≡Fe^{III} + L	⇄	≡Fe^{III}L		$1.0\cdot10^{5}$ / $3.0\cdot10^{5}$ (a)	(R1a)
≡Fe^{III}L	→	≡ + Fe^{III}L		3.5×10^{-5} (b) / 3.5×10^{-5} (a)	(R1b)
≡ + bulk	→	≡Fe^{III}		1×10^{8} / 1×10^{8} (c)	(R1c)
Photochemical formation of Fe(II) and oxidants					
Lp	$-h\nu$, bulk LMCT →	*Lp-bulk-h^{+}* + *Lp-bulk-e^{-}*		-	(R2a)
Lp-bulk-h^{+} + *Lp-bulk-e^{-}*	→	*≡Fe^{IV}* + *≡Fe^{II}*		-	(R2b)
bulk	$h\nu$ →	≡Fe^{IV} + ≡ Fe^{II}		$6.5\cdot10^{-6}$ / $2.7\cdot10^{-6}$ (d)	(R2ab)
≡Fe^{IV} + ≡Fe^{II}	→	bulk		-	(R2c)
≡Fe^{IV} (+OH^{-})	→	≡Fe^{III} + ≡$^{\bullet}$OH		$1.0\cdot10^{6}$ (c)	(R2d)
≡$^{\bullet}$OH + ≡$^{\bullet}$OH	→	H_2O_2		$1.6\cdot10^{3}$ / $8.7\cdot10^{3}$ (d)	(R2e)
≡Fe^{IV} + L	→	≡Fe^{III} + L$^{\bullet}$		-	(R2f)
≡Fe^{III}L	$h\nu$ →	≡Fe^{II} + L$^{\bullet}$		-	(R2g)
≡Fe^{II} + bulk	→	≡Fe^{III}-O-Fe^{II}		1×10^{8} (c)	(R2h)
Adsorption and desorption of Fe^{II}					
≡Fe^{III} + Fe^{II}	⇄	≡Fe^{III}-O-Fe^{II}		$7.2\cdot10^{6}$ / $7.2\cdot10^{6}$ (a)	R3
Fe(II)-catalyzed dissolution					
≡Fe^{III}-O-Fe^{II} + L	→	≡Fe^{II} + Fe^{III}L		95 (b) / 61 (a)	(R4a)
≡Fe^{III} + Fe^{II}L	→	≡Fe^{II} + Fe^{III}L		$6.0\cdot10^{2}$ / $1.4\cdot10^{2}$ (a)	(R4b)
≡Fe^{III}L + Fe^{II}	→	≡Fe^{II} + Fe^{III}L		- / $2.2\cdot10^{4}$ (a)	(R4c)
≡Fe^{II} + bulk	→	≡Fe^{III}-O-Fe^{II}		1×10^{8} / 1×10^{8} (c)	(R4d)
Formation of dissolved complexes					
Fe^{II} + L	⇄	Fe^{II}L		$6.0\cdot10^{11}$ / $5.3\cdot10^{4}$ (a)	(R5)
Oxidation of surface Fe(II) by H_2O_2 and by dissolved O_2					
≡Fe^{III}-O-Fe^{II} + H_2O_2	→	bulk + $^{\bullet}$OH		$4.3\cdot10^{2}$ / $2.1\cdot10^{3}$ (d)	(R6a)
≡Fe^{III}-O-Fe^{II} + (O_2)	→	bulk + $^{\bullet}O_2^{-}$		$6.4\cdot10^{-3}$ / $1.1\cdot10^{-3}$ (e)	(R6b)
Photolysis of dissolved Fe(III)L (only for Fe^{III}EDTA)					
Fe^{III}-L	$h\nu$ →	Fe^{II} + L$^{\bullet}$		1.2×10^{-4} / 1×10^{-9} (f)	(R7a)
Fe^{II} (+ O_2)	→	$Fe^{III}(OH)_3$		$1\cdot10^{-3}$ (b)	(R7b)
L$^{\bullet}$ (+ O_2)	→	P + $^{\bullet}O_2^{-}$		$1\cdot10^{5}$ (b)	(R7c)
O_2^{-} + O_2^{-}	→	H_2O_2 + (O_2)		$1\cdot10^{7}$ (b)	(R7d)
L + $^{\bullet}$OH	→	L$^{\bullet}$ + OH^{-}		*$1\cdot10^{9}$* (c)	(R7e)
H_2O_2 + Fe^{II}	→	$^{\bullet}$OH + $Fe^{III}(OH)_3$		$1\cdot10^{3}$ (b)	(R7f)
Formation and reactions of oxidants					
≡Fe^{II} + $^{\bullet}$OH	→	→ ≡Fe^{III} + (OH^{-})		$1.0\cdot10^{1}$ / $1.0\cdot10^{1}$ (b)	(R8a)
L + ≡$^{\bullet}$OH	→	L$^{\bullet}$		$1.0\cdot10^{1}$ / $1.0\cdot10^{1}$ (b)	(R8b)

In this list, L stands for EDTA or DFOB. Reactants written in parentheses are present at constant concentrations (e.g. O_2 at 250 µM under aerated conditions and <10 nM under anoxic conditions). They are not entered explicitly in the model, but are contained in the corresponding pseudo-first order reaction rate coefficients. OH^{-} and H^{+} are also present at constant concentrations and are not listed as reactants and products. The reactions are thus not balanced for charge, OH^{-}, H^{+}, and H_2O. As dissolved and adsorbed ligands are present in the form of several differently protonated species – and the speciation of surface species is uncertain – inclusion of all equations with dissolved and adsorbed species is not possible. The listed rate coefficients are thus conditional rate coefficients for pH 7.0 and the other specific conditions in this system. The initial bulk concentration of Lp and Gt were 1.13 mM; the concentration of surface sites was 8.5 µM (the same as in (Biswakarma et al., 2020) and close to the 8.3 µM surface sites for adsorption of EDTA in (Biswakarma et al., 2019)).

[a] Rate coefficients and equilibria constants from (Biswakarma et al., 2020) for DFOB. The rate coefficients

µM) used in this model. (Where only footnote is indicated, it applies for both values).

[b] Adjusted rate coefficients.

[c] Fast, non-rate-determining rate coefficients.

[d] Rate coefficients for the photochemical production of Fe(II) were calculated from the rates of formation of Fe(II) in Table 1a. With the bulk concentration of 1.13 M, the rate coefficients were 480 $nMmin^{-1}/(60s\ min^{-1} \cdot 1.13mM) = 6.35\ \mu s^{-1}$ for EDTA, and 180 $nMmin^{-1}/(60\ s\ min^{-1} \cdot 1.13mM) = 2.65\ \mu s^{-1}$.

[e] Adjusted rate coefficient for the oxidation of adsorbed Fe(II).

[f] Rate coefficient for the photolysis of dissolved Fe(III)EDTA from the rates listed in Table 1a (column 6).

Reactions for which no rate coefficients are stated (indicated by a dash), were not used in the model. The rate coefficients listed here are for the fits shown in Figures 2 and 3. Rate coefficients for all fits are listed in Table S3b.

In Table 2b, we list degradation reactions of EDTA in more detail. Similar reactions can occur with DFOB, but they are less important because dissolved complexes of DFOB are photostable and far less degraded, even during continuous illumination. To obtain good fits to our data, the reactions listed in Table 2a were sufficient.

Table 2b. List of addional possible reactions shown in more detail with EDTA

Reaction					
Photochemical Fe(II) formation with EDTA as hole scavenger					
$\equiv Fe^{IV}$ + EDTA	→	$\equiv Fe^{III}$ + ED3A'-$CH_2COO^{\bullet}$			(R9a)
$\equiv Fe^{III}$ +ED3A'-$CH_2COO^{\bullet}$ + OH^-	→	$\equiv Fe^{II}$ +CO_2 + CH_2O + ED3A			(R9b)
ED3A'-$CH_2COO^{\bullet}$ + O_2 (+ OH^-)	→	CO_2 + CH_2O + ED3A + $^{\bullet}O_2^-$			(R9c)
Photochemical Fe(II) formation with adsorbed EDTA as chromophore					
$\equiv Fe^{III}$-EDTA	hν→	$\equiv Fe^{II}$ + $^{\bullet}$OOC-CH_2-ED3A'			(R10a)
$\equiv Fe^{III}$ +ED3A'-$CH_2COO^{\bullet}$ + OH^-		$\equiv Fe^{II}$ + CH_2O + CO_2 + ED3A			(R10b)
Reactions of EDTA with $^{\bullet}$OH or $\equiv Fe^{III}$-O-Fe^{IV}					
EDTA + $^{\bullet}$OH	→	ED3A'-$CH_2COO^{\bullet}$			(R11a)
EDTA + $\equiv Fe^{IV}$	→	ED3A'-$CH_2COO^{\bullet}$ + $\equiv Fe^{III}$			(R11b)
ED3A'-$CH_2COO^{\bullet}$ + O_2	→	CO_2 + CH_2O + ED3A + $^{\bullet}O_2^-$			(R11c)
Photolysis of dissolved Fe^{III}EDTA complexes					
Fe^{III}EDTA	hν→	Fe^{II} + ED3A'-$CH_2COO^{\bullet}$			R12a
ED3A'-$CH_2COO^{\bullet}$ + O_2 (+ OH^-)	→	ED3A + CO_2 + CH_2O + $^{\bullet}O_2^-$			R12b

EDTA stands for the fully deprotonated (ethylenediaminetetraacetate) and differently protonated species. We do not specify the charges of dissolved and surface complexes to keep the list of reactions short and due to the uncertain structures and charges of surface complexes. Several differently protonated and charged complexes contribute to each reaction.

We used the following abbreviations and notations:
EDTA: $(C_2H_4N_2)(CH_2\text{-}COO)_4^{4-}$
ED3A': $(C_2H_4N_2)(CH_2\text{-}COO)_3^{3-}$
ED3A: $(C_2H_4N_2H)(CH_2\text{-}COO)_3^{3-}$
In the kinetic model (Table 2a) ED3A'-$CH_2COO^{\bullet}$ is abbreviated as $^{\bullet}$L, ED3A is abbreviated as P.
For DFOB we used the same abbreviations, but the structure of $^{\bullet}$L and P are not specified. As mentioned above, DFOB is degraded less than EDTA, and an exact description of its degradation was not required for good model fits.

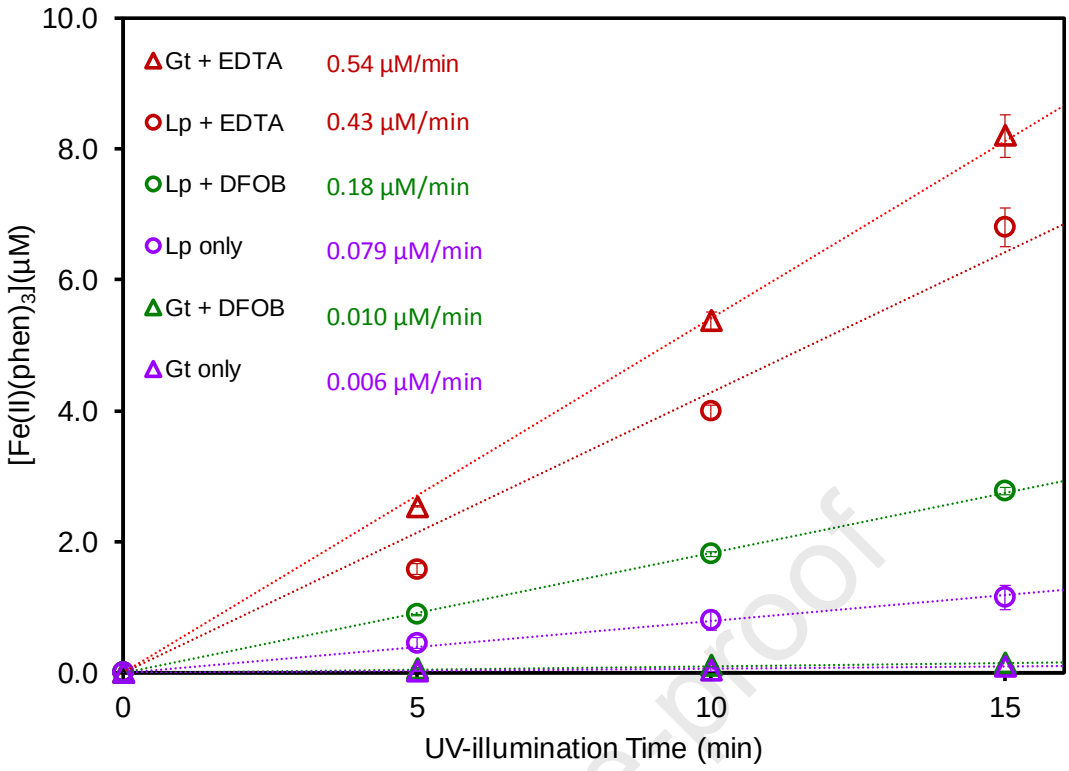

Figure 1. Cummulative Fe(II) production as a function of total illumination time. Fe(II) was produced in three 5 min illumination intervals (30-35 min, 60-65min, 90-95 min) in 1.13 mM lepidocrocite (Lp) and goethite (Gt) suspensions. Photoproduced Fe(II) was measured with phenanthroline in the absence of other ligands, and in the presence of 50 μM EDTA or DFOB at pH 7.0 (carbonate buffer; anoxic). Error bars correspond to the range of duplicate measurements. Solid lines represent linear fits. The measurement with Lp and DFOB is shown in more detail in Fig. S3.

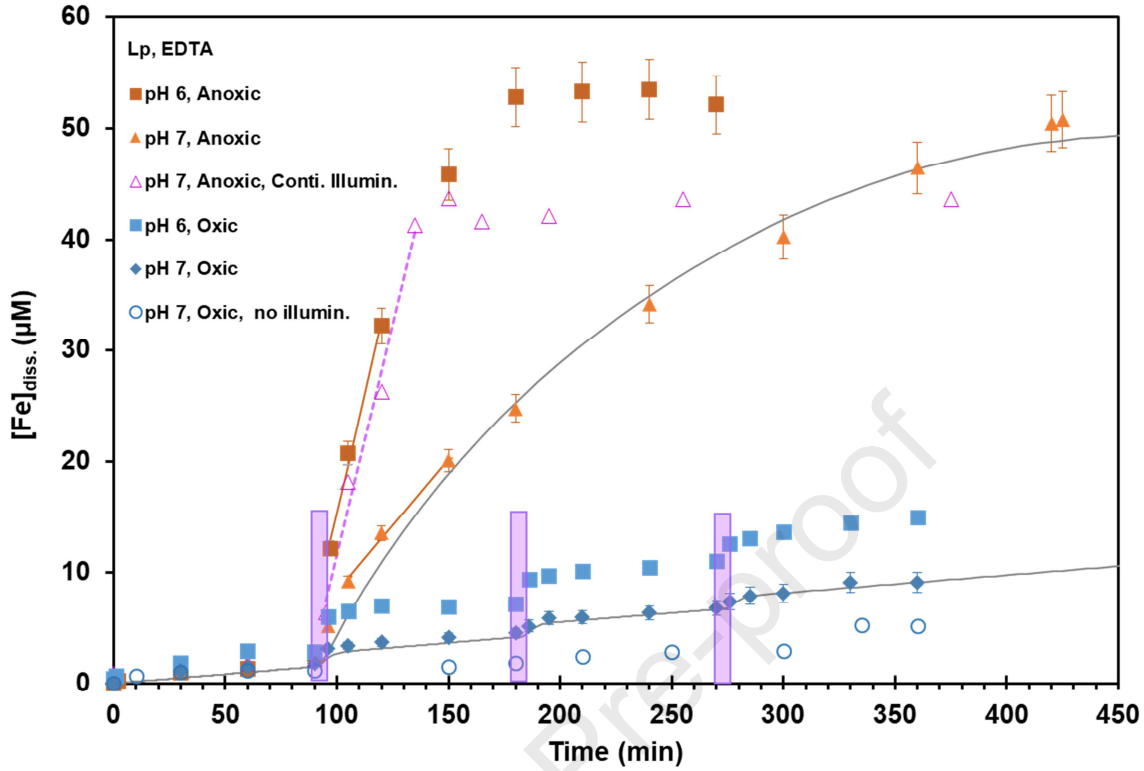

Figure 2. Lp dissolution in the presence of 50 µM EDTA. UV-A intermittent illumination intervals of 5 min (shown by purple bars) applied to Lp (1125 µM) suspension at pH 6 and 7. A single illumination (90-95 min) was applied under anoxic conditions, and three intermittent illuminations (90-95, 180-185, 270-275 min) were applied under oxic conditions. Also shown are data (purple triangles) with continuous illumination at pH 7. After 5 min illumination, accelerated Lp dissolution (anoxic) occurred rapidly until all free ligand was complexed with Fe in the dark. In contrast, Lp dissolution under oxic conditions was not faster after illumination than before illumination, at both pH 6 and 7. Slopes were determined from the liner fits to the data points, as shown by solid lines. The thin black lines are the output of the kinetic model where the model was re-started when conditions changed as explained in the text using reactions and parameters listed in Table 2.

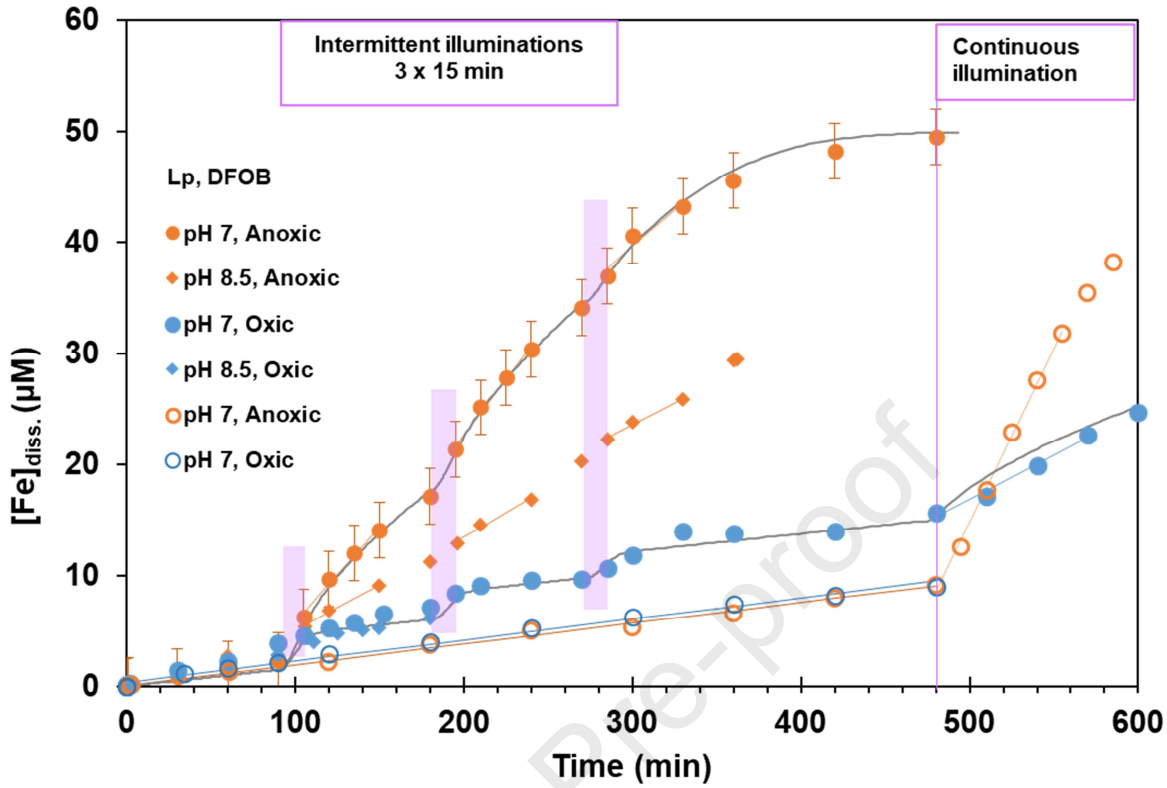

Figure 3. Lp dissolution in the presence of 50 µM DFOB. Three intermittent illuminations with UV-A of 15 min each, are indicated with purple bars (90-105, 180-195, 270-285 min). Fe_{diss} was formed at accelerated rates after intermittent illuminations under anoxic (orange symbols), but not under oxic (blue symbols) conditions, both at pH 7.0 and pH 8.5. Note that no data was collected during intermittent illumination. The open circles from 0-480 min show Lp-dissolution in the dark under anoxic and oxic conditions. Continuous illumination from 480-600 min at pH 7 without prior illumination under anoxic conditions (open orange circles) and after prior intermittent illuminations under oxic conditions (filled blue circles) led to accelerated dissolution. The acceleration was by a factor of 2-3 larger under the anoxic condition. Colored solid lines represent the linear fits to selected data points for slope determination. The thin black lines are the output of the kinetic model as explained in caption for Figure 2.

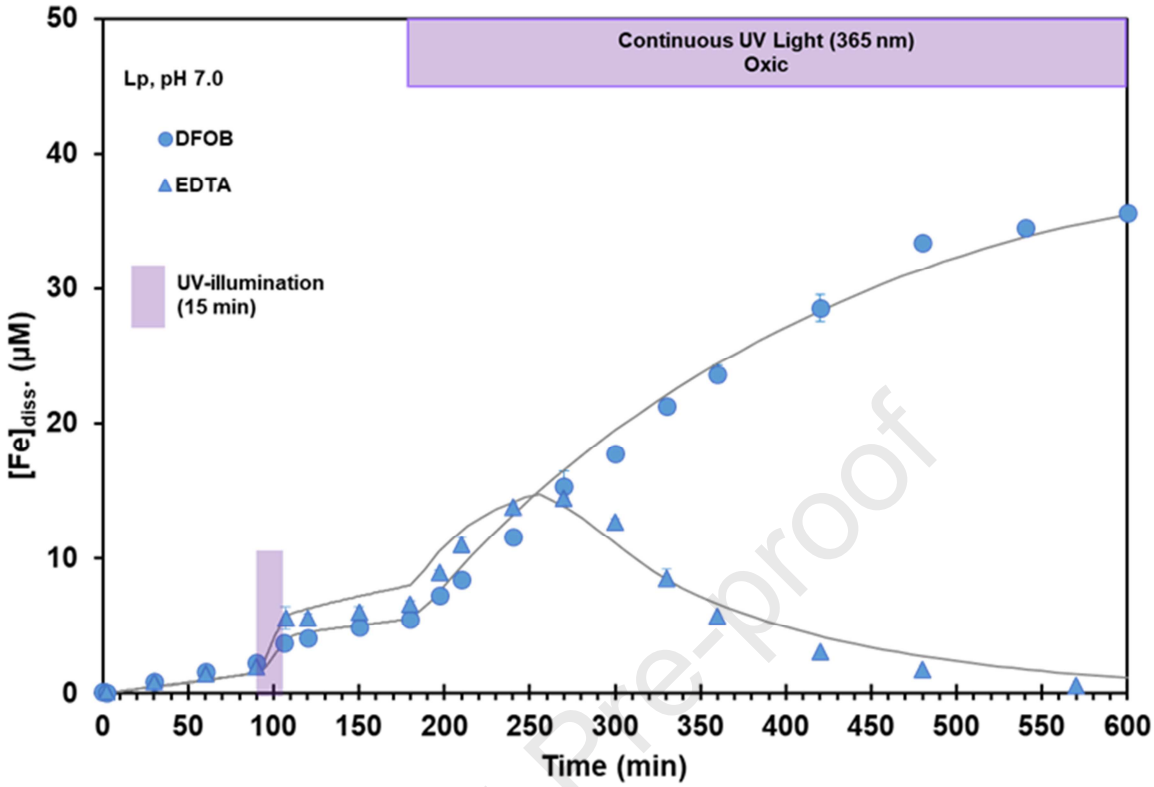

Figure 4. Lp dissolution (oxic; pH 7.0) in the presence of 50 µM DFOB or EDTA. One intermittent illumination from 90-105 min is indicated by a purple bar. From 180-600 min, continuous illumination was applied. Lp dissolution with DFOB continued in the light, indicating that Fe(III)DFOB complexes are not or only slowly photolyzed. With EDTA, $[Fe]_{diss}$ declines rapidly after 280 min, due to photolysis of Fe(III)EDTA complexes and degradation of EDTA. Error bars up to 420 min correspond to the range of duplicate measurements, data points from 450-600 min are from single measurements. The thin black lines are the output of the kinetic model as explained in caption for Figure 2.

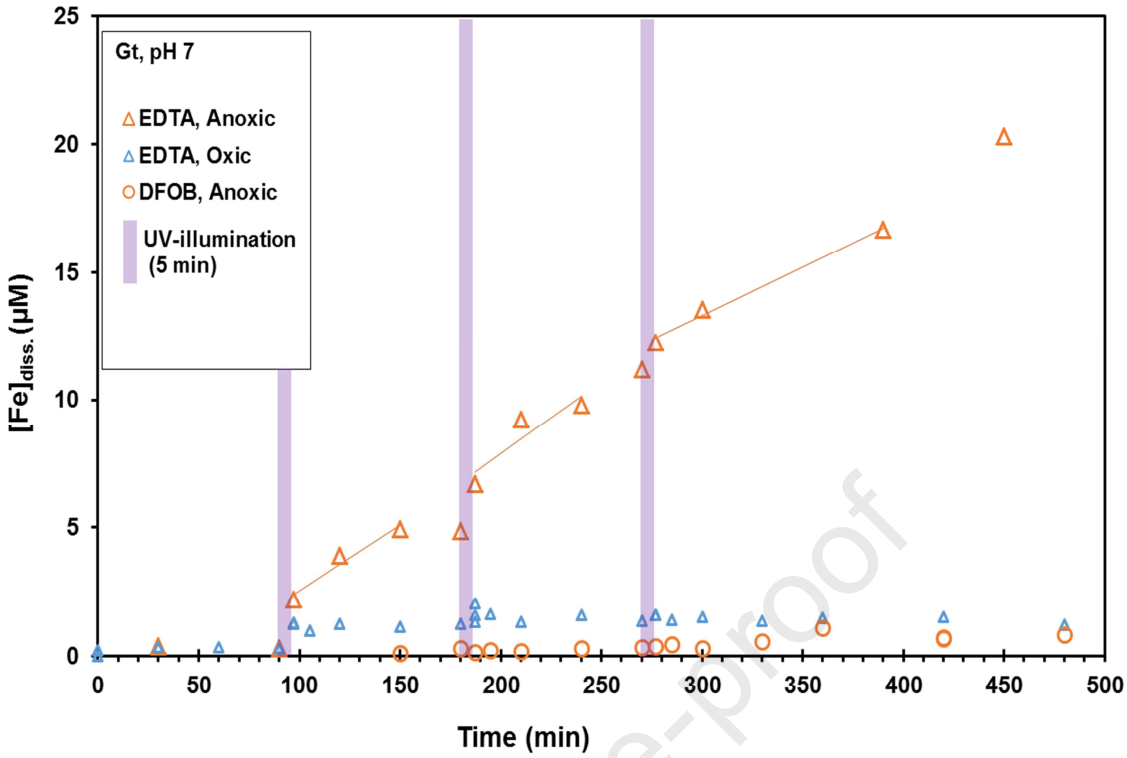

939

940 **Figure 5.** Goethite dissolution in the presence of 50 µM EDTA or DFOB at pH 7.0. Intermittent
941 illumination intervals with UV-A, indicated with purple bars, were applied from 90-95, 180-185, 270-
942 275 min. Lines represent the linear fits to the data. Intermittent illumination led to accelerated
943 dissolution in the dark only in the presence of EDTA under anoxic condition. With DFOB, $[Fe]_{diss}$
944 remained too low for the determination of dissolution rates even under anoxic condition and was not
945 measurable under oxic conditions.

946

947

948

Declaration of Competing Interest

The authors declare that they have no known competing financial interests or personal relationships that could have appeared to influence the work reported in this paper.

CRediT authorship contribution statement

Jagannath Biswakarma: Conceptualization, Methodology, Investigation, Writing - original draft. **Kyounglim Kang:** Conceptualization, Investigation, Contribution to final document. **Walter D.C. Schenkeveld:** Conceptualization, Review & editing, Funding acquisition. **Stephan M. Kraemer:** Conceptualization, Review & editing, Funding acquisition. **Janet G. Hering:** Conceptualization, Supervision, Review & editing, Funding acquisition. **Stephan J. Hug:** Conceptualization, Methodology, Supervision, Writing - review & editing, Funding acquisition, Project administration.